Tellus A
Dynamic Meteorology and Oceanography

Analytical Formulas for the Structure of Perturbations in the Eady Model of Baroclinic Instability in the *p*-System

ORIGINAL RESEARCH PAPER

STOCKHOLM UNIVERSITY PRESS

ALEŠ RAIDL
HYNEK BEDNÁŘ
JIŘÍ MIKŠOVSKÝ

*Author affiliations can be found in the back matter of this article

ABSTRACT

Shortly after World War II, the first two models of baroclinic instability were independently published by Charney (1947) and Eady (1949). Both authors describe the origin and initial development of midlatitude weather disturbances from infinitesimal perturbations of a certain initial state of the atmosphere. In this paper we focus on the latter model (Eady, 1949). Using the normal mode method, we derive analytical formulas for the structure of perturbations in the field of geopotential, temperature, isobaric divergence, and vertical velocity. We work in the p coordinate system, in contrast to the original Eady study and its modifications. This allows us to not limit ourselves to the troposphere but to introduce a natural boundary condition at the upper boundary of the atmosphere. The derived analytical relationships accurately well describe some aspects of synoptic disturbances in the midlatitudes. We focus particularly on the wavelength of disturbances, their vertical structure, the position of the minimum divergence level, and the growth rate of emerging synoptic disturbances.

CORRESPONDING AUTHOR:
Aleš Raidl
Department of Atmospheric Physics, Faculty of Mathematics and Physics, Charles University, Prague, Czech Republic
ales.raidl@mff.cuni.cz

KEYWORDS:
baroclinic instability; Eady model; perturbations; analytical structure

TO CITE THIS ARTICLE:
Raidl, A., Bednář, H. and Mikšovský, J. (2025) Analytical Formulas for the Structure of Perturbations in the Eady Model of Baroclinic Instability in the *p*-System. *Tellus A: Dynamic Meteorology and Oceanography*, 77(1): 136–150. DOI: https://doi.org/10.16993/tellusa.4077

1 INTRODUCTION

According to modern concepts of dynamic meteorology, the mechanism of baroclinic instability is responsible for the genesis and development of synoptic-scale weather disturbances in the midlatitudes (Holton, 2004). This process is called cyclogenesis. In its basic features, this problem can be described within the framework of quasi-geostrophic theory, in which perturbations in the form of normal modes are superimposed on the basic state (most simply zonal flow). Under appropriate atmospheric conditions, perturbations can grow from their essentially infinitesimal amplitude into wave disturbances, and their subsequent transformation can give rise to synoptic-scale disturbances. From an energy point of view, this process represents a situation in which the available potential energy of the basic state is transferred to the energy of the perturbations, primarily to the available potential energy of the disturbances, which is further transformed into their kinetic energy. Baroclinic instability is related to the vertical gradient of wind velocity and through the thermal wind relation (see e.g., Holton, 2004; Bluestein, 1993) to the horizontal gradient of temperature.

The first studies of baroclinic instability were carried out independently by Charney (1947) and Eady (1949). Both authors worked with a vertically continuous model of the atmosphere and made several simplifications. In addition, Eady used simplifications in the atmosphere (e.g., f-plane) such that the problem could be solved analytically in an illustrative way.

In this paper, we derive explicit analytical relationships for wave-like perturbations in the fields of geopotential, temperature, isobaric divergence, and vertical velocity. In contrast to other analyses of the Eady model, we work with pressure as the vertical coordinate, i.e., in the p-system. This allows us to place the upper boundary condition at the upper boundary of the atmosphere for p approaching zero. Note that in the original Eady paper and later modifications (e.g., Haltiner and Williams, 1980; Holton, 2004; Pedlosky, 1987), the upper rigid boundary is placed at a finite height above the ground surface, which most often simulates the position of the tropopause. The use of the p-system allows us to naturally incorporate Earth's surface topography.

In this article, we do not aim to provide a comprehensive overview of the various aspects of baroclinic instability. For this purpose, we refer to the existing monographs (e.g., Holton, 2004; Pedlosky, 1987; North et al., 2015; Grotjahn, 1993; Mak, 2011). The reader should also pay attention to the necessary condition for baroclinic instability by Charney and Stern (1962). Although Eady's original work was published many years ago, the related topics are still actively researched, with recent relevant studies including Kalashnik and Chkhetiani (2018), Stamper and Taylor (2017) or Vic, Carton and Gula (2022).

2 BASIC EQUATIONS

The subject of our interest will be baroclinic instability on synoptic to planetary scales. The motions of such a scale can be described by the vorticity equation in the quasi-geostrophic approximation and by the thermodynamic equation in the adiabatic approximation:

$$\frac{\partial}{\partial t}\nabla_p^2\psi + \boldsymbol{v}_\psi \cdot \nabla_p\left(\nabla_p^2\psi + f\right) = f_0\frac{\partial \omega}{\partial p}, \tag{1}$$

$$\frac{\partial}{\partial t}\left(\frac{\partial \psi}{\partial p}\right) + \boldsymbol{v}_\psi \cdot \left(\frac{\partial \psi}{\partial p}\right) + \frac{\sigma\omega}{f_0} = 0, \tag{2}$$

where t is time, $\boldsymbol{v}_\psi = \boldsymbol{k} \times \nabla_p\psi$ is the velocity vector of the non-divergent flow, ψ represents the stream function, and f_0 is the value of the Coriolis parameter f at the reference mean latitude φ_0, usually chosen as 45° N. It is clear from both Eqs. (1) and (2) we will continue to work in the p-system (standard coordinate system with p as vertical coordinate). Thus, ω has the meaning of the vertical velocity in the p-system, $\omega = dp/dt$; ∇_p is gradient in p-system; and σ represents parameter of static stability of the atmosphere (see Appendix for the definition). We refer the reader who is not familiar with the derivation of these equations to any of the following references: Holton (2004); Dutton (1986); Haltiner and Williams (1980). We remark that in the following we will assume a simplified geostrophic relationship between the geopotential ϕ and the stream function $\phi = f_0\psi$.

After some simple modifications, Eqs. (1) and (2) can be used to obtain

$$\frac{\partial}{\partial t}\left[\nabla_p^2\psi + f_0\frac{\partial}{\partial p}\left(\frac{1}{\sigma}\frac{\partial \psi}{\partial p}\right)\right] + \boldsymbol{v}_\psi \cdot \nabla_p\left[\nabla_p^2\psi + f + f_0\left(\frac{1}{\sigma}\frac{\partial \psi}{\partial p}\right)\right] = 0. \tag{3}$$

In the last equation, we can denote

$$\Pi = \nabla_p^2\psi + f + f_0^2\frac{\partial}{\partial p}\left(\frac{1}{\sigma}\frac{\partial \psi}{\partial p}\right). \tag{4}$$

We call the quantity Π the quasi-geostrophic potential vorticity and Eq. (3) is the quasi-geostrophic potential vorticity equation.

We assume that the state of the atmosphere can be decomposed into a basic state and at least an order of magnitude smaller perturbation. We will denote the basic state by a bar and the perturbation by a comma. Let the basic state be the purely zonal flow described by the geostrophic stream function $\bar{\psi}(y, p)$, which corresponds to the velocity of zonal flow

$$U = -\frac{\partial \bar{\psi}}{\partial y}(y, p). \tag{5}$$

The perturbation stream function is $\psi'(x, y, p, t)$, $|\psi'| \ll |\bar{\psi}|| \psi'| \ll |\bar{\psi}|$. The resulting flow is then characterized by the stream function

$$\psi(x, y, p, t) = \bar{\psi}(y, p) + \psi'(x, y, p, t). \tag{6}$$

By substituting Eqs. (5) and (6) into Eq. (3), we obtain

$$\left(\frac{\partial}{\partial t}+U\frac{\partial}{\partial x}\right)q'+\frac{\partial \psi'}{\partial x}\frac{\partial \bar{\Pi}}{\partial y}+J\left(\psi',q'\right)=0, \tag{7}$$

where J is Jacobian and

$$q'=\nabla_p^2\psi'+f_0^2\frac{\partial}{\partial p}\left(\frac{1}{\sigma}\frac{\partial \psi'}{\partial p}\right), \tag{8}$$

is the perturbation potential vorticity. Quantity

$$\frac{\partial \bar{\Pi}}{\partial y}=\beta-\frac{\partial^2 U}{\partial y^2}-f_0^2\frac{\partial}{\partial p}\left(\frac{1}{\sigma}\frac{\partial U}{\partial p}\right) \tag{9}$$

represents the meridional gradient of the potential vorticity of the base state $\bar{\Pi}$,

$$\bar{\Pi}=\nabla_p^2\bar{\psi}+f+f_0^2\frac{\partial}{\partial p}\left(\frac{1}{\sigma}\frac{\partial \bar{\psi}}{\partial p}\right), \tag{10}$$

and $\beta=\partial f/\partial y$ is the Rossby parameter describing the meridional variation of the Coriolis parameter f, arising from the sphericity of the Earth (American Meteorological Society, 2025).

Since we consider all perturbation quantities to be at least an order of magnitude smaller in absolute value than their corresponding basic state quantities, we can neglect the terms in Eq. (7) that are nonlinear with respect to the perturbations in the first approximation. That is, we neglect the Jacobian $J(\psi',q')$. This is an important assumption, as it allows us to only consider the "small enough" perturbations, i.e., those in the early stages of development. The linearized form of the potential vorticity equation of perturbations is then

$$\left(\frac{\partial}{\partial t}+U\frac{\partial}{\partial x}\right)q'+\frac{\partial \psi'}{\partial x}\frac{\partial \bar{\Pi}}{\partial y}=0. \tag{11}$$

The solution of this equation is found in the waveform

$$\psi'=Re[\hat{\psi}(y,p)e^{ik(x-ct)}], \tag{12}$$

where Re denotes the real part of the expression it precedes by and c is the phase speed, which can be complex (c = c_r + ic_i; i denotes the imaginary unit $i=\sqrt{-1}$), k is the wave number and $\hat{\psi}$) is the amplitude. In the following, the Re marker will be omitted for brevity. Substituting the last expression into Eq. (11), we get

$$(U-c)\left[\frac{\partial^2\hat{\psi}}{\partial y^2}-k^2\hat{\psi}+f_0^2\left(\frac{1}{\sigma}\frac{\partial\hat{\psi}}{\partial p}\right)\right]+\frac{\partial \bar{\Pi}}{\partial y}\hat{\psi}=0. \tag{13}$$

Analogously, we modify Eq. (2) by substituting from Eqs. (5) and (6). After that, we obtain

$$\left(\frac{\partial}{\partial t}+U\frac{\partial}{\partial x}\right)\frac{\partial \psi'}{\partial p}-\frac{\partial \psi'}{\partial x}\frac{\partial U}{\partial p}+J\left(\psi',\frac{\partial \psi'}{\partial p}\right)+\frac{\sigma\omega}{f_0}=0. \tag{14}$$

We linearize Eq. (14) again by neglecting the Jacobian $J(\psi',\frac{\partial\psi'}{\partial p})$ and we introduce the wave expression for the vertical velocity in the p-system into this equation

$$\omega=\hat{\omega}(p)e^{ik(x-ct)}, \tag{15}$$

where $\hat{\omega}$ is amplitude of ω. Using Eqs. (5), (12) and (15), the linearized Eq. (14) takes the form

$$ik(U-c)\frac{\partial\hat{\psi}}{\partial p}-ik\frac{\partial U}{\partial p}\hat{\psi}+\frac{\sigma\hat{\omega}}{f_0}=0. \tag{16}$$

Thus, we have obtained two relations, Eqs. (13) and (16), for the amplitudes $\hat{\psi}$ and $\hat{\omega}$ of the wave solutions.

3 THE BAROCLINIC INSTABILITY OF THE CONTINUOUS MODEL ON THE *f* PLANE

We now study the baroclinic instability using an Eady-type model, but with some modifications compared with the original work (Eady, 1949). The main change is that we will work in a p-system, thus avoiding the need to introduce a boundary condition on the rigid upper boundary of the atmosphere, as was done in the original article (Eady, 1949).

We start from Eqs. (13) and (16). Recall that we formulated the thermodynamic equation Eq. (16) for the case of adiabaticity of the processes described. We will further assume that the static stability parameter of the atmosphere σ does not change with height and that the atmosphere is vertically stably stratified. Thus, for the parameter of static stability, which we will refer to as $\bar{\sigma}$, we have $\sigma\equiv\bar{\sigma}=const>0$. Let the basic zonal flow velocity U be a linear function of the vertical coordinate p, and the solutions of Eqs. (13) and (16) independent of latitude, i.e., the amplitude of the perturbation is $\hat{\psi}\neq\hat{\psi}(y)$. Finally, we disregard the change in the Coriolis parameter by setting $\beta=0$, therefore f will be constant and equal to f_0. By introducing these assumptions, we simplify the model enough to find its analytical solution, but not so much that the solution obtained loses a substantial connection with the real atmosphere. As we will see later, the assumption of the constant value of the Coriolis parameter is most important for the stability of perturbations.

With these assumptions, the meridional gradient of the potential vorticity of the basic state, Eq. (9), is equal to zero, $\frac{\partial\bar{\Pi}}{\partial y}=0$, and the equation of the potential vorticity, Eq. (13), goes into the form

$$(U-c)\left(\frac{f_0^2}{\bar{\sigma}}\frac{d^2\hat{\psi}}{dp^2}-k^2\hat{\psi}\right)=0. \tag{17}$$

In last equation, in accordance with the assumptions, let us put

$$U=S(p_0-p),\quad S=const>0,\quad p_0=1000\text{hPa}. \tag{18}$$

The nonsingular solution of Eq. (17) has the form

$$\hat{\psi} = A\cosh(ap) + B\sinh(ap) \tag{19}$$

where A and B are constants and

$$a \equiv \frac{k}{f_0}\sqrt{\bar{\sigma}}. \tag{20}$$

The thermodynamic equation, Eq. (16), is used to include the boundary conditions for the generalized vertical velocity ω, or its amplitude $\hat{\omega}$. Specifically, for $p = p_0$ and $p = 0$, we obtain from Eq. (16)

$$(U-c)\frac{d\hat{\psi}}{dp} - \frac{dU}{dp}\hat{\psi} = 0. \tag{21}$$

By inserting Eqs. (18), (19) and (20) into Eq. (21) we obtain a system of two homogeneous algebraic equations

$$SA + a(Sp_0 - c)B = 0, \tag{22a}$$

$$[S\cosh(ap_0) - ca\sinh(ap_0)]A + [S\sinh(ap_0) - ca\cosh(ap_0)]B = 0, \tag{22b}$$

that have a nontrivial solution just when the determinant of its coefficients is equal to zero:

$$\begin{vmatrix} S & a(Sp_0 - c) \\ S\cosh(ap_0) - ca\sinh(ap_0) & S\sinh(ap_0) - ca\cosh(ap_0) \end{vmatrix} = 0.$$

The calculation of this determinant leads to a quadratic equation for the phase speed c

$$a^2c^2 - a^2Sp_0c + S^2[ap_0\coth(ap_0) - 1] = 0, \tag{23}$$

the solution of which yields the expression

$$c = \frac{Sp_0}{2} \pm \frac{Sp_0}{2}\sqrt{1 - \frac{4}{p_0^2a^2}[ap_0\coth(ap_0) - 1]}. \tag{24}$$

Using the identity

$$\coth x = \frac{1}{2}\left(\tanh\frac{x}{2} + \coth\frac{x}{2}\right),$$

Eq. (24) takes the more elegant form

$$c = \frac{Sp_0}{2} \pm \frac{S}{a}\sqrt{\left(\frac{p_0a}{2} - \tanh\frac{p_0a}{2}\right)\left(\frac{p_0a}{2} - \coth\frac{p_0a}{2}\right)}. \tag{25}$$

Since $\frac{p_0a}{2} > \tanh\frac{p_0a}{2}$ for all values of a, the expression under the square root in Eq. (25) is positive if $\frac{p_0a}{2} > \coth\frac{p_0a}{2}$. In such a case, the phase speed c would be real and the perturbation in our model would be stable. However, we will be particularly interested in the opposite case. The term under the square root in Eq. (25) is equal to zero if

$$\frac{p_0a}{2} = \coth\frac{p_0a}{2}, \tag{26a}$$

which is true for

$$\frac{p_0a}{2} = 1.1997. \tag{26b}$$

This result was obtained by numerical calculation. Substituting Eq. (20) into Eq. (26b) and using the relationship between the wavenumber k and the wavelength L, $k = 2\pi/L$, we obtain an expression for the critical wavelength

$$L_c = \frac{\pi\sqrt{\bar{\sigma}}p_0}{1.1997f_0} \doteq 2.542 \cdot 10^9\sqrt{\bar{\sigma}}, \tag{27}$$

where we use $p_0 = 10^5$ Pa and $f_0 = 1.03 \cdot 10^{-4}$ s^{-1}. The interpretation of the critical wavelength L_c is evident from how we obtained the relationship for its calculation. For all perturbations with a wavelength L shorter than L_c, the term below the square root in Eq. (25) is positive and the phase speed c is a real number – we get two perturbations with a non-variable amplitude. Conversely, if $L > L_c$, the expression below the square root in Eq. (25) is negative, and thus the phase speed c has a non-zero imaginary part – we have two perturbations with variable amplitude, one of which increases with increasing time and the other that decreases with increasing time. If we set $\bar{\sigma} = 2 \cdot 10^{-6} m^2s^{-2}Pa^{-2}$, L_c is 3 595 km. The chosen value $\bar{\sigma}$ is the mean value of the static stability parameter between the 1 000 and 350 hPa levels at a temperature drop of 0.65 K per 100 m and a temperature of 288 K at the 1 000 hPa level – see the Appendix for more information. Eq. (27) shows an interesting finding: for a fixed latitude φ_0(and thus $f_0 = 2\Omega\sin\varphi_0$) the critical wavelength depends only on the stability of the vertical stratification of the atmosphere, so that with increasing stability the value of L_c moves to longer wavelengths. At a fixed value of $\bar{\sigma}$ and as the distance from the equator (as well as f_0) increases, L_c becomes shorter.

The real part of the phase speed c_r is shown in Figure 1. To obtain it, we put $S = 2.5 \cdot 10^{-4}$ ms^{-1}Pa^{-1} $\bar{\sigma}$ and chose the same as in the previous paragraph – we use the same values for both parameters in the following text, unless explicitly stated otherwise. From Figure 1, we can see that the two perturbations move with variable amplitudes at different speeds, which converge when the wavelength of the two perturbations approaches the critical wavelength of L_c. Perturbations with variable amplitude then move with the same speed, which depends on the vertical gradient of the flow velocity S and is equal to $c_r = \frac{Sp_0}{2}$. Considering Eq. (18), we see that this is also the speed of the basic flow U_{500} at the level of 500 hPa. This level is therefore the steering level of our model (see also Pedlosky, 1987).

From Eq. (25) we also determine the growth rate kc_i of unstable amplifying perturbations:

$$kc_i = \frac{kS}{a}\sqrt{\left(\frac{p_0a}{2} - \tanh\frac{p_0a}{2}\right)\left(\coth\frac{p_0a}{2} - \frac{p_0a}{2}\right)}. \tag{28}$$

The same value of kc_i, but with the opposite sign, is reached by perturbations whose amplitude decreases with time. The evolution of kc_i as a function of wavelength is shown in Figure 2. It clearly shows the position of the critical wavelength L_c and that the short-wavelength perturbations are stable, while for $L > L_c$ there are perturbations with increasing amplitude.

Note that there is a wavelength, denoted L_D, for which the growth rate is maximum. This means that there is a perturbation that grows fastest in our linear approach and thus starts to dominate the perturbation field after a certain time. This perturbation with wavelength L_D will therefore be called the dominant perturbation or disturbance. Figure 2 indicates that growth rate of dominant perturbation is approximately $5.5 \cdot 10^{-6}\ s^{-1}$ and the corresponding *e*-folding time is about 2.1 days. Let us calculate the value of L_D. To do this, we need to solve the equation

$$\frac{d}{dk}(kc_i) = 0, \qquad (29)$$

which, after substitution by Eq. (28) and derivation, leads to the equation

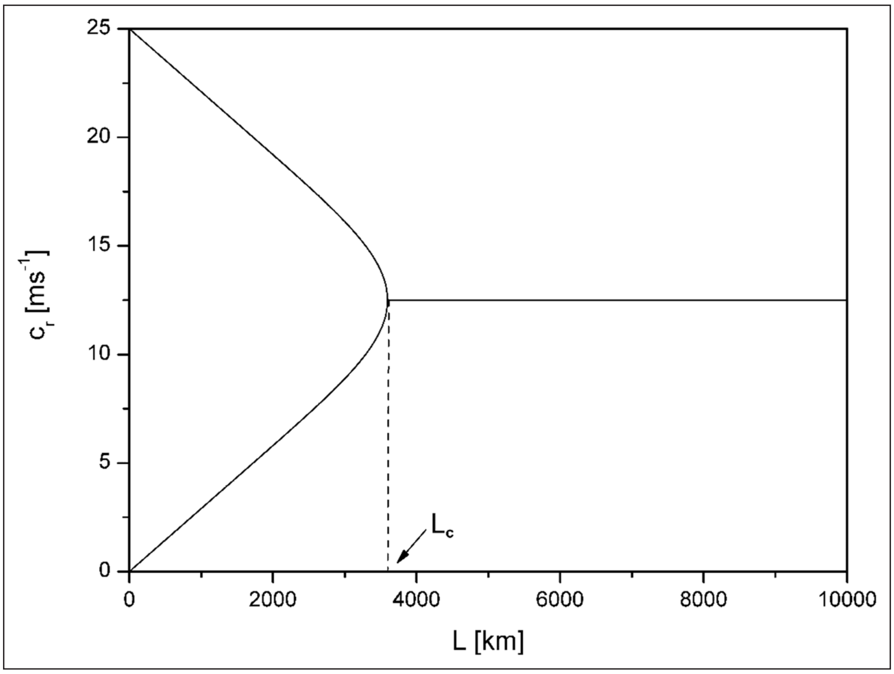

Figure 1 The dependence of the real part of the phase speed c_r on the wavelength L of disturbances. L_c denotes the critical wavelength.

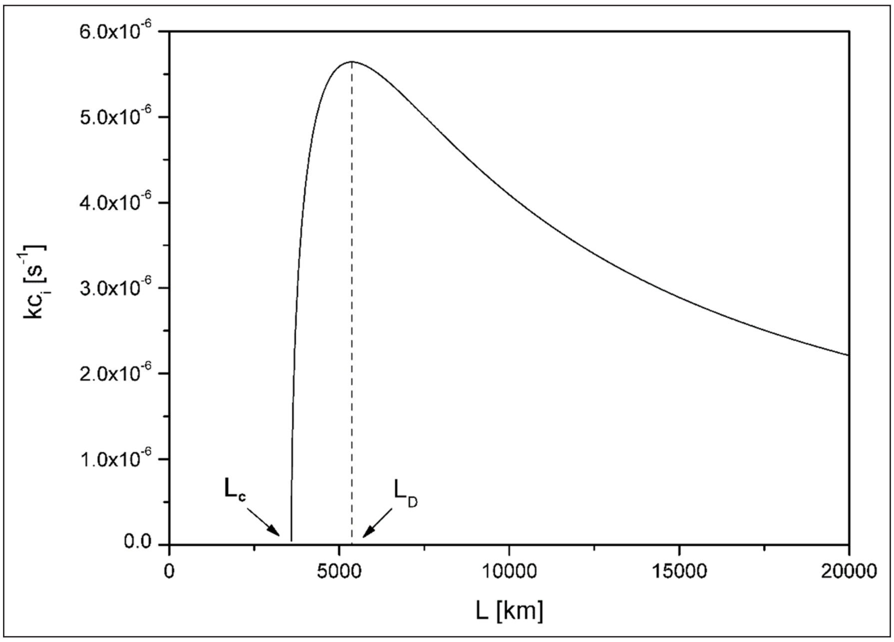

Figure 2 The dependence of the growth rate kc_i of the perturbations on the wavelength L. L_D denotes the wavelength of the dominant perturbation, L_c is the critical wavelength.

$$\coth\frac{p_0a}{2}-\frac{p_0a}{2sinh^2\frac{p_0a}{2}}+\tanh\frac{p_0a}{2}+\frac{p_0a}{2cosh^2\frac{p_0a}{2}}-p_0a=0. \quad (30)$$

The numerical solution of Eq. (30) gives

$$\frac{p_0a}{2}=0.8031, \quad (31)$$

from which, after substituting from the Eq. (26b) and using $k=\frac{2\pi}{L}$, we obtain the expression for the wavelength of the dominant perturbation:

$$L_D=\frac{\pi\sqrt{\bar{\sigma}}p_0}{0.8031f_0}\doteq 3.798\cdot 10^9\sqrt{\bar{\sigma}}. \quad (32)$$

We used the same values of p_0 and f_0 in calculating the approximate Eq. (32) as in the calculation of the critical wavelength L_c. By comparing the Eqs. (32) and (27), we see that the wavelength of the dominant perturbation has similar properties to L_c, i.e., it increases with increasing stability of the vertical stratification of the atmosphere and decreases with increasing distance from the equator. After all, as the formulas for L_D and L_c show, the two wavelengths are linked by a definite relationship $L_D \doteq 1.49384L_c$. If $\bar{\sigma}=2\cdot 10^{-6}m^2s^{-2}Pa^{-2}$ is selected again, the L_D is 5,300 km. As said before, perturbation with this wavelength will dominate the spectrum of increasing perturbations after a certain period, according to the chosen linear approach. If we consider that a quarter of the wavelength of the perturbation corresponds to the distance of the high-pressure ridge from the low-pressure trough, it follows $\frac{L_D}{4}\approx 1\,000$ km. This agrees very well with the characteristic magnitude of the synoptic-scale disturbances in the midlatitudes. Our model of baroclinic instability thus captures the origin of these synoptic disturbances reasonably well, even within the linear approximation, and with several simplifying assumptions made.

4 VERTICAL STRUCTURE OF UNSTABLE PERTURBATIONS

4.1 GEOPOTENTIAL PERTURBATIONS

In the next part of the text, we focus on determining the structure of unstable (growing) perturbations, especially of the dominant perturbation. From Eq. (22a), we express the constant B and substitute into Eq. (19) to obtain an expression for the amplitudes of the perturbation stream function:

$$\hat{\psi}=Acosh(ap)-\frac{AS}{a(Sp_0-c)}sinh(ap). \quad (33a)$$

However, we are unable to determine the constant A within the framework of linear theory, so in the following we set it equal to one. Keep in mind that the amplitudes obtained can be multiplied by a real non-zero constant, so instead of the last relation we will write

$$\hat{\psi}=cosh(ap)-\frac{S}{a(Sp_0-c)}sinh(ap). \quad (33b)$$

Thanks to Eq. (12), the perturbation stream function can be expressed as

$$\psi'=\left[cosh(ap)-\frac{S}{a(Sp_0-c)}sinh(ap)\right]e^{ik(x-ct)}. \quad (34a)$$

Since we used a simplified relationship between the geopotential and the stream function $\phi=f_0\psi$, in deriving the potential vorticity Eq. (13), which became the starting point for the present considerations, Eqs. (33) also represent the formulas for the amplitude or perturbation in the geopotential field, except for the multiplier f_0:

$$\hat{\varphi}=f_0\left[cosh(ap)-\frac{S}{a(Sp_0-c)}sinh(ap)\right], \quad (33c)$$

$$\varphi'=f_0\left[cosh(ap)-\frac{S}{a(Sp_0-c)}sinh(ap)\right]e^{ik(x-ct)}. \quad (34b)$$

If we decompose the phase speed of instable disturbances into a real and imaginary part

$$c=c_r+ic_i=\frac{Sp_0}{2}+ic_i, \quad (35)$$

and if we substitute this decomposition into Eq. (33c), we obtain:

$$\hat{\varphi}=f_0\left[cosh(ap)-\frac{S}{a\left(\frac{Sp_0}{2}-ic_i\right)}sinh(ap)\right]. \quad (36)$$

We modify the second term in the square bracket of the last expression as follows:

$$\frac{1}{\left(\frac{Sp_0}{2}-ic_i\right)}\frac{\left(\frac{Sp_0}{2}+ic_i\right)}{\left(\frac{Sp_0}{2}+ic_i\right)}=\frac{Sp_0}{2\left(\frac{S^2p_0^2}{4}+c_i^2\right)}+i\frac{c_i}{\left(\frac{S^2p_0^2}{4}+c_i^2\right)}.$$

For the amplitude of the geopotential perturbations, we thus have

$$\hat{\varphi}=f_0\left[cosh(ap)-\frac{S^2p_0}{2a\left(\frac{S^2p_0^2}{4}+c_i^2\right)}sinh(ap)-i\frac{Sc_i}{a\left(\frac{S^2p_0^2}{4}+c_i^2\right)}sinh(ap)\right], \quad (37)$$

and by choosing $\hat{\varphi}=|\hat{\varphi}|e^{i\alpha_\varphi}$, where α_ϕ is the phase angle, we can write

$$\varphi'=e^{kc_it}|\hat{\varphi}|e^{i(kx+\alpha_\varphi-kc_rt)}, \quad (38)$$

where $c_r = \frac{Sp_0}{2}$ and further that

$$|\hat{\varphi}| = f_0 \sqrt{\left[cosh(ap) - \frac{S^2 p_0 sinh(ap)}{2a\left(\frac{S^2 p_0^2}{4} + c_i^2\right)}\right]^2 + \left[\frac{Sc_i sinh(ap)}{a\left(\frac{S^2 p_0^2}{4} + c_i^2\right)}\right]^2}, \quad (39)$$

$$\mathrm{tg}\alpha_\varphi = \frac{-2Sc_i sinh(ap)}{2a\left(\frac{S^2 p_0^2}{4} + c_i^2\right)cosh(ap) - S^2 p_0 sinh(ap)}. \quad (40)$$

Again, recall that only the real part of Eq. (38) is physically meaningful. The vertical plot of the absolute value of the perturbation amplitude $|\hat{\varphi}|$ in the geopotential field for the dominant disturbance is shown in Figure 3a. We see that the amplitude reaches maximum values at the surface and at the upper boundary of the atmosphere, while it is at its minimum at 500 hPa. The formula (40) shows that for an unstable disturbance the phase angle changes with the vertical coordinate – for a growing perturbation it increases with height, which means that the growing perturbation in the field of geopotential tilts towards the west with increasing height, thus against the direction of the base eastward flow U (see Eq. (18)). In other words, this means that a strengthening perturbation in the geopotential field near the Earth's surface precedes the perturbation in the higher levels of the atmosphere. This lead depends on the wavelength $L > L_c$. More detailed calculation can show that for a strengthening wave disturbance with a wavelength of 4,000 km, this lead between the levels of 1,000 and 500 hPa slightly exceeds 20°, while for a disturbance with a wavelength of 7,000 km, the lead is only 10°. Isolines of constant phase satisfy the following relationship at any moment:

$$kx = -\alpha_\phi(p) + const. \quad (41)$$

The profile of the phase angle α_ϕ with vertical coordinate for the dominant perturbation is shown in Figure 4a. It is also clear from Eq. (40) that weakening perturbations tilt towards the east in the geopotential field with increasing height, i.e., in the opposite direction to strengthening perturbations.

4.2 TEMPERATURE PERTURBATIONS

Perturbations in the temperature field are determined by the equation of hydrostatic equilibrium

$$\frac{\partial \varphi'}{\partial p} = -\alpha' = -\frac{RT'}{p} \quad (42)$$

that is

$$T' = -\frac{p}{R}\frac{\partial \varphi'}{\partial p}, \quad (43)$$

R is the gas constant for dry air, R = 287 J kg^{-1}K^{-1}. By substituting Eq. (34b) into these last Eqs. and using $e^{i\pi} = -1$, we can write

$$T' = \frac{f_0 p}{R}\left[asinh(ap) - \frac{S}{Sp_0 - c}cosh(ap)\right]e^{i(kx+\pi-kct)}. \quad (44)$$

Considering Eq. (34b) it follows that perturbations with time-invariant amplitude are mutually shifted by 180° in the geopotential and temperature fields. If we consider

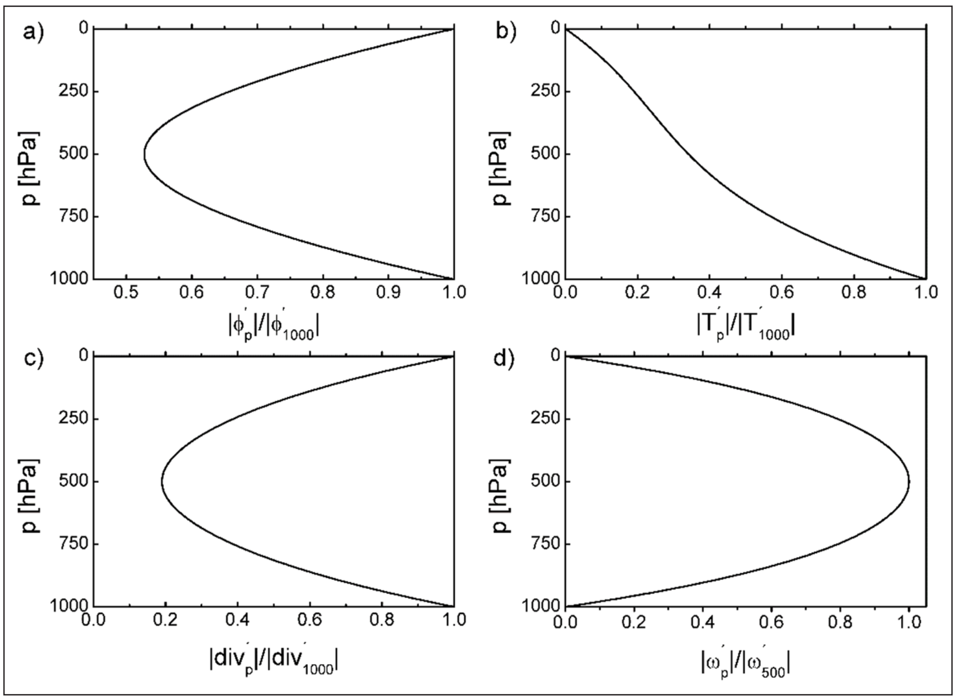

Figure 3 Vertical profile of amplitude of the dominant perturbation in the geopotential **(a)**, temperature **(b)**, isobaric divergence **(c)**, and generalized vertical velocity **(d)**.

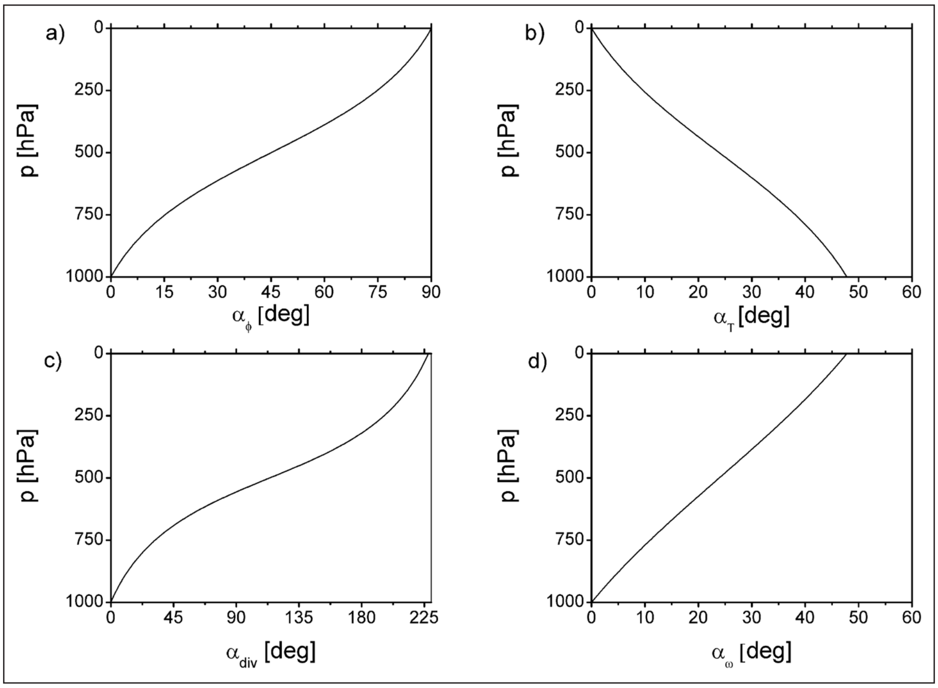

Figure 4 Vertical profile of phase angle of dominant perturbation in the geopotential **(a)**, temperature **(b)**, isobaric divergence **(c)**, and generalized vertical velocity **(d)**.

the increasing perturbations and decompose the phase speed c by Eq. (35), we obtain for perturbations in the temperature field

$$T' = \frac{f_0 p}{R}\left[\frac{S^2 p_0}{2\left(\frac{S^2 p_0^2}{4}+c_i^2\right)}\cosh(ap) - a\sinh(ap) + i\frac{Sc_i}{\left(\frac{S^2 p_0^2}{4}+c_i^2\right)}\cosh(ap)\right]e^{ik(x-ct)}. \quad (45)$$

By using a similar procedure as in the expression for φ' (Eq. (38)) we obtain

$$T' = e^{kc_i t}\,|\hat{T}|\,e^{i(kx+\alpha_T - kc_r t)}, \quad (46)$$

where

$$|\hat{T}| = \frac{f_0 p}{R}\sqrt{\left[\frac{S^2 p_0 \cosh(ap)}{2\left(\frac{S^2 p_0^2}{4}+c_i^2\right)} - a\sinh(ap)\right]^2 + \left[\frac{Sc_i\cosh(ap)}{\left(\frac{S^2 p_0^2}{4}+c_i^2\right)}\right]^2}, \quad (47)$$

and

$$\mathrm{tg}\alpha_T = \frac{2Sc_i\cosh(ap)}{S^2 p_0\cosh(ap) - 2a\sinh(ap)\left(\frac{S^2 p_0^2}{4}+c_i^2\right)}. \quad (48)$$

Due to the decrease in pressure and air density with height, the amplitude $|\hat{T}|$ decreases with height, in accordance with Eq. (47) – see Figure 3b. Thus, perturbations in the temperature field are most pronounced at the surface. As for the phase angle, for increasing perturbations this angle α_T decreases with increasing height and the isolines of the constant phase in the temperature perturbation field slope towards the east, i.e., in the opposite direction to the geopotential. The vertical profile α_T for the dominant perturbation is shown in Figure 4b.

4.3 ISOBARIC DIVERGENCE PERTURBATIONS

Perturbations in the field of isobaric divergence in the p-system, $\nabla_p \cdot v'$, are determined using the vorticity equation (Eq. (1)), which for perturbations under the given assumptions switches to the form

$$\frac{\partial}{\partial t}\frac{\partial^2\psi'}{\partial x^2} + U\frac{\partial}{\partial x}\frac{\partial^2\psi'}{\partial x^2} = f_0\frac{\partial\omega}{\partial p}. \quad (49)$$

The continuity equation in the p-system can be expressed as

$$\nabla_p \cdot v' + \frac{\partial\omega}{\partial p} = 0. \quad (50)$$

By combining the last two equations with respect to Eq. (12) and rearranging, we obtain

$$\nabla_p \cdot v' = \frac{ik^3}{f_0}(U-c)\hat{\psi}(p)e^{ik(x-ct)}. \quad (51)$$

Using Eq. (35) and analogous modifications as in the derivation of Eqs. (38) and (46) after some calculations we arrive at the expression

$$\nabla_p \cdot v' = e^{kc_i t}\,|\hat{D}|\,e^{i(kx+\alpha_D - kc_r t)}, \quad (52)$$

where

$$|\hat{D}| = \frac{1}{f_0}\left\{\left[k^3 S\left(\frac{p_0}{2}-p\right)D_1\sinh(ap) + k^3 c_i\left(\cosh(ap) - D_2\sinh(ap)\right)\right]^2 + \left[k^3 S\left(\frac{p_0}{2}-p\right)\left(\cosh(ap) - D_2\sinh(ap)\right) - k^3 c_i D_1\sinh(ap)\right]^2\right\}^{1/2}, \quad (53)$$

$$\mathrm{tg}\alpha_D = \frac{S\left(\frac{p_0}{2}-p\right)\left[\cosh(ap)-D_2\sinh(ap)\right]-c_iD_1\sinh(ap)}{S\left(\frac{p_0}{2}-p\right)D_1\sinh(ap)+c_i\left[\cosh(ap)-D_2\sinh(ap)\right]}, \tag{54}$$

$$D_1 = \frac{Sc_i}{a\left(\frac{S^2p_0^2}{4}+c_i^2\right)}, \quad D_2 = \frac{S^2p_0}{2a\left(\frac{S^2p_0^2}{4}+c_i^2\right)}. \tag{56}$$

The vertical profile of the amplitude $|\hat{D}|$ for the dominant perturbation is shown in Figure 3c. It is clear from this that we observe the minimum, but not zero, divergence at the 500 hPa level. This agrees relatively well with the conditions in the real atmosphere, in which the level of minimum divergence is situated in the vicinity of the 500 hPa. The dependence of the phase angle α_D on the vertical coordinate for the given perturbation is shown in Figure 4c. The isolines of the constant phase α_D tilt westward with height, so they have the same direction as the perturbations in the geopotential field. The difference is that α_D has a larger range than α_ϕ. The tilt of perturbations in the isobaric divergence field is therefore greater than in the geopotential field. In fact, it is also greater than for perturbations in the temperature field and the generalized vertical velocity ω, as we will see later.

4.4 VERTICAL VELOCITY PERTURBATIONS

Let us now describe the structure of the vertical velocities in our model. By substituting $\hat{\omega}$ into Eq. (15) using the thermodynamic Eq. (16), in which we express $\partial U/\partial p = -S$, we can give the generalized vertical velocity in p-system in the form

$$\omega = -\frac{ikf_0}{\bar{\sigma}}\left[(U-c)\frac{d\hat{\psi}}{dp}+S\hat{\psi}\right]e^{ik(x-ct)}. \tag{57}$$

Using Eq. (33b) for the perturbation stream function, expressing Eq. (18), and performing similar modifications as in the derivation of Eqs. (38), (46) or Eq. (52), after some modifications we arrive at the following expression for the generalized vertical velocity:

$$\omega = e^{kc_it}\,|\hat{\omega}|\,e^{i(kx+\alpha_\omega-kc_rt)}, \tag{58}$$

where

$$\begin{aligned}|\hat{\omega}| = \frac{f_0k}{\bar{\sigma}}\Bigg\{&\Bigg[ac_i\left(D_2\cosh(ap)-\sinh(ap)\right)\\&-aSD_1\left(\frac{p_0}{2}-p\right)\cosh(ap)-SD_1\sinh(ap)\Bigg]^2\\&+\Bigg[aS\left(\frac{p_0}{2}-p\right)\left(D_2\cosh(ap)-\sinh(ap)\right)\\&-aD_1c_i\cosh(ap)+S\left(D_2\sinh(ap)-\cosh(ap)\right)\Bigg]^2\Bigg\}^{\frac{1}{2}},\end{aligned} \tag{59}$$

$$\mathrm{tg}\alpha_\omega = \frac{aS\left(\frac{p_0}{2}-p\right)\left[D_2\cosh(ap)-\sinh(ap)\right]-aD_1c_i\cosh(ap)+S\left[D_2\sinh(ap)-\cosh(ap)\right]}{ac_i\left[D_2\cosh(ap)-\sinh(ap)\right]-aSD_1\left(\frac{p_0}{2}-p\right)\cosh(ap)-SD_1\sinh(ap)}. \tag{60}$$

The parameters D_1 and D_2 are given by Eqs. (56). The vertical profile of the $|\hat{\omega}|$ amplitude for the dominant perturbations is shown in Figure 3d. It shows that the most intense vertical movements are registered at the level of 500 hPa, which, after all, we could infer from the knowledge of the $\nabla_p \cdot \mathbf{v}'$ isobaric divergence field distribution. The vertical profile of the phase angle α_ω for the dominant perturbation can be seen again in Figure 4d. This figure shows that the phase angle increases with height, so the isolines of constant phase in the field of generalized vertical velocity tilt towards the west, i.e., against the direction of the basic zonal flow. We arrive at the same situation as we have observed for perturbations in the geopotential field and isobaric divergence.

5 VERTICAL CROSS-SECTION OF THE DOMINANT PERTURBATION

An illustrative view of the mutual arrangement of the individual fields of geopotential, temperature, isobaric divergence, and generalized vertical velocity of perturbations, for which we derived analytical relationships above, provides information about the position of the extrema of these fields at each pressure level. Extrema in the geopotential and temperature fields are determined using the following conditions:

- maximum:

$$kx+\alpha_\varphi = 0+2\pi n,$$
$$kx+\alpha_T = 0+2\pi n, \quad n = \ldots,-1,0,1,\ldots \tag{61a}$$

- minimum:

$$kx+\alpha_\varphi = \pi+2\pi n,$$
$$kx+\alpha_T = \pi+2\pi n, \quad n = \ldots,-1,0,1,\ldots \tag{61b}$$

The arrangement of these extremes for the dominant disturbance is shown in Figure 5a. Realizing that ϕ_{max}, or ϕ_{min}, represents the axis of a high-pressure ridge (or anticyclone), or the axis of a low-pressure trough (or cyclone), respectively, it is clear that the surface area of low pressure represents a warm formation with the warmest zone in its frontal part, while the area of high pressure at the ground surface is a cold formation with the coldest air again in front of its surface axis. With increasing altitude, the warm air approaches the high-pressure ridge and the cold air approaches the low-pressure trough. From the above facts and from Figure 5a, it is therefore clear that the geopotential and temperature perturbation fields are not in phase, but rather the geopotential wave precedes the temperature wave. In the steering level of 500 hPa, this lead is 90°, or 1/4 wavelength.

The profiles of the extremes in the field of isobaric divergence $\nabla_p \cdot v'$ and vertical motion w can be determined in a similar way:

maximum:

$$kx + \alpha_D = 0 + 2\pi n,$$
$$kx + \alpha_\omega = 0 + 2\pi n, \quad n = \ldots -1, 0, 1, \ldots \tag{62a}$$

minimum:

$$kx + \alpha_D = \pi + 2\pi n,$$
$$kx + \alpha_\omega = \pi + 2\pi n, \quad n = \ldots, -1, 0, 1, \ldots \tag{62b}$$

The configuration of these extremes is shown in Figure 5b. We can see that at the ground surface, the area of minimum isobaric divergence, which is actually maximum convergence $\nabla_p \cdot v' < 0$ is accompanied by maximum upward air motion ω_{min}, while in the area of the upper atmosphere, the opposite is true – the area of maximum isobaric convergence of flow velocity corresponds to the maximum of downward motion at the upper atmosphere boundary. By analogy, the maximum of isobaric divergence at the surface is associated with the maximum of downward air motions; at the upper boundary of the atmosphere the situation is again reversed, with the maximum of isobaric divergence of the flow velocity coinciding with the maximum region of outward air motions.

Comparing Figure 5a and 5b, we find that in the surface low pressure area, isobaric divergence of the flow dominates along with upward air motion. Note further that the most intense upward air motion is located at the 500 hPa level (see Figure 4d), and at this level the maximum upward motion precedes the surface axis of the low-pressure area by 45°, which corresponds to 1/8 of the wavelength of the disturbance. Therefore, if we hypothetically consider the possibility of water vapor condensation and precipitation, according to our model we would expect the location of the most intense precipitation to be at a distance of approximately $\frac{L}{8}$ ahead of the surface axis of the pressure trough, which for dominant perturbation corresponds to a distance of approximately 660 km.

A comprehensive view of the structure of the most rapidly intensifying perturbation is provided by Figures 6, 7, 8 and 9, which show the perturbations in the geopotential field (Figure 6), temperature (Figure 7), isobaric divergence (Figure 8), and generalized vertical velocity (Figure 9) for one and a quarter wavelengths of the L_D. All four figures essentially confirm the previously presented results. At this point, however, it should be pointed out that our temperature perturbations pattern in Figure 7 differs from the isolines of the temperature perturbations published by Holton (2004, Figure 8.10 page 259), who also analyzed the Eady-type model. The Holton temperature perturbations have the same amplitude at the lower and upper boundaries of the model. However, Holton (2004) followed Eady (1949)

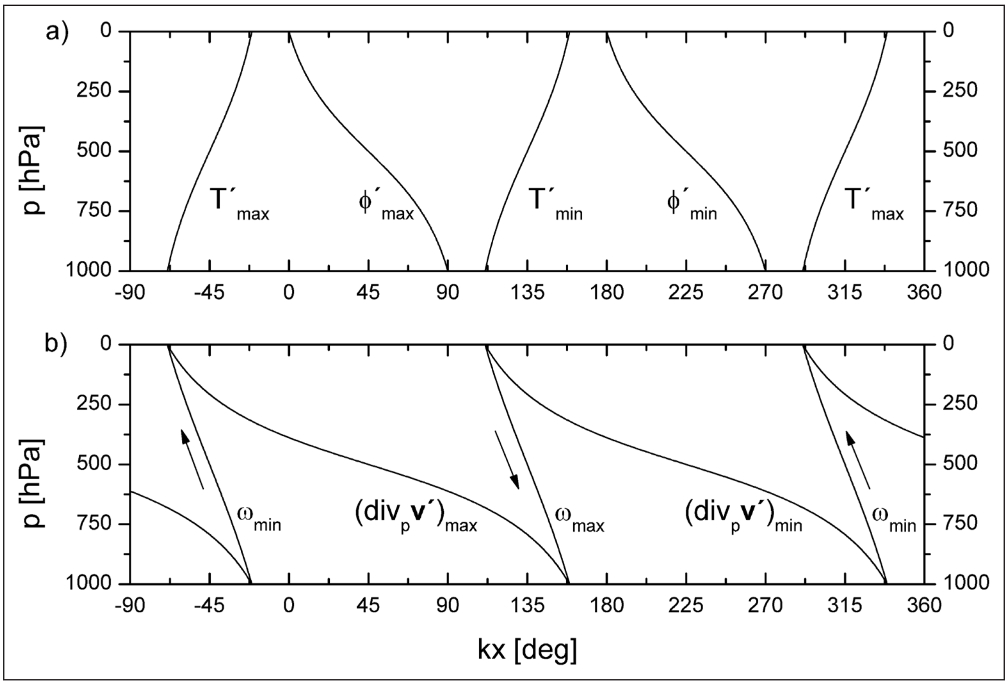

Figure 5 Positions of maxima and minima of the dominant perturbation in the geopotential and temperature fields **(a)**, and isobaric divergence and generalized vertical velocity fields **(b)**.

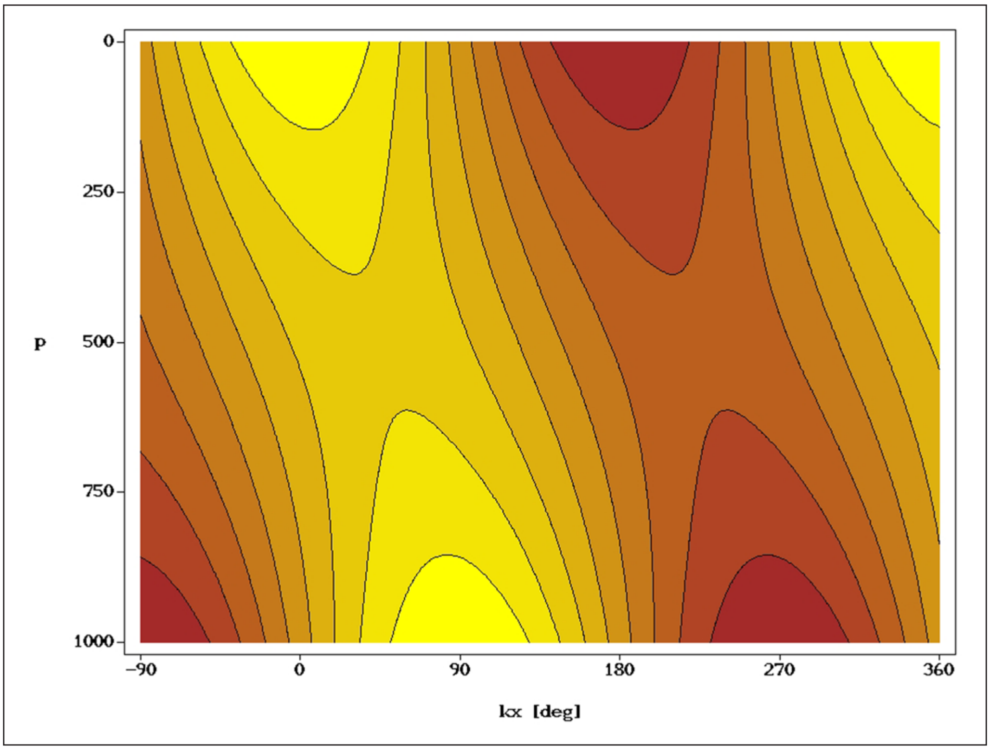

Figure 6 The geopotential field of the dominant perturbation. The high-pressure region is shown in yellow, the low-pressure region in brown.

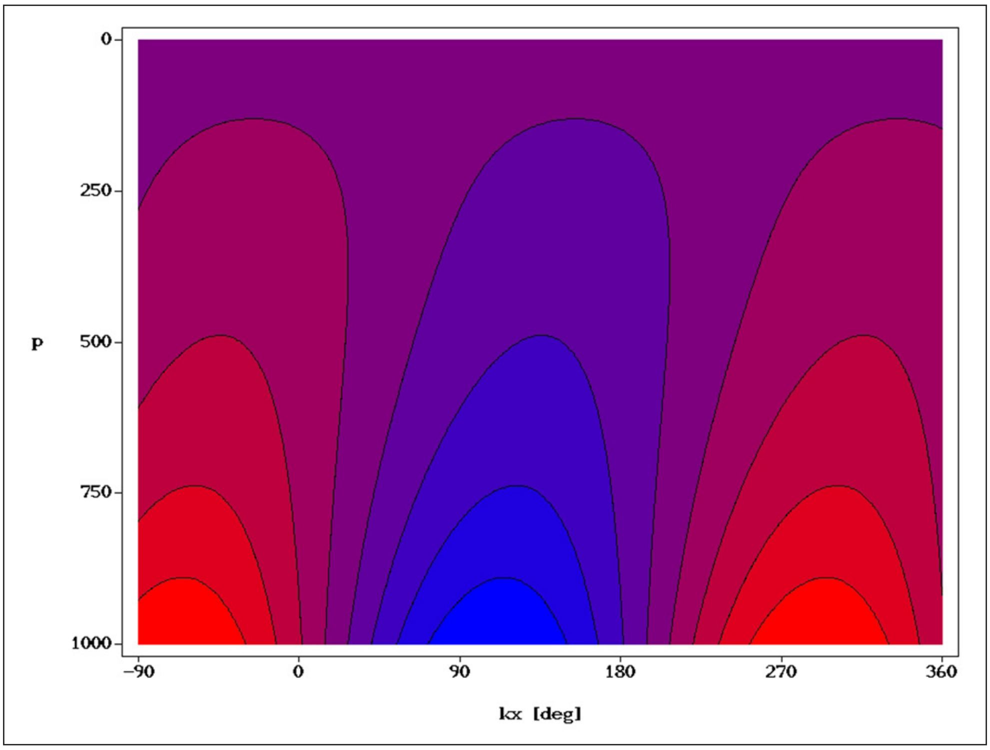

Figure 7 Temperature field of the dominant perturbation. The coldest air region is plotted in blue, the warm air region in red.

more closely, in that he constrained the model by two rigid boundaries at heights $z = 0$ and $z = H < \infty$ and worked with the height z as the vertical coordinate. In our opinion, our modification of the Eady model and the use of the p-system better corresponds to the conditions in the real atmosphere.

CONCLUDING REMARKS

It was demonstrated that despite using a relatively simple model, we were able to capture some of the key properties of real synoptic-scale disturbances in the midlatitudes,

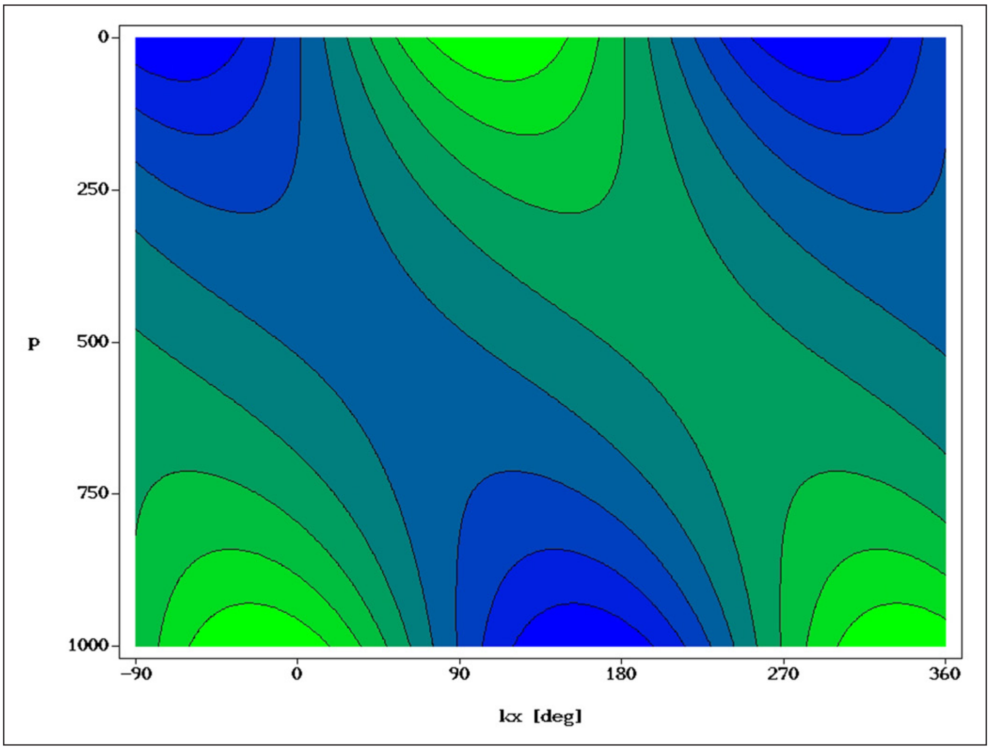

Figure 8 The isobaric divergence field of the dominant perturbation. The region of isobaric divergence is plotted in blue, the region of isobaric convergence in green.

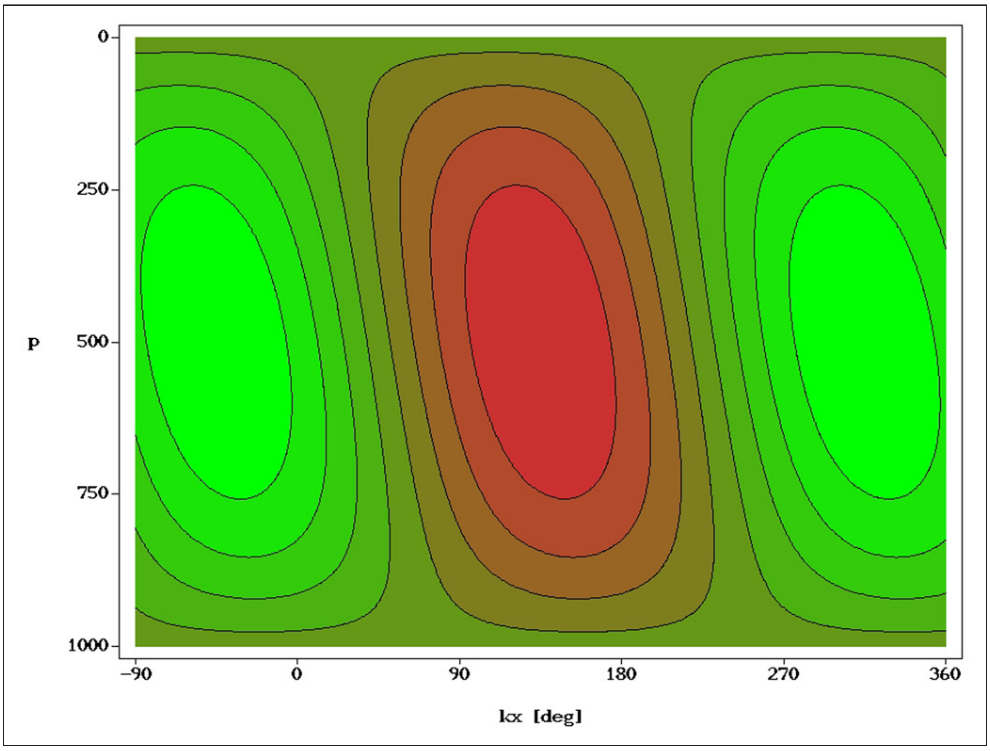

Figure 9 The generalized vertical velocity field of the dominant perturbation. The region of downward motions is plotted in brown, the region of upward motions in green.

primarily in the early stages of their development, due to the linearization of the governing equations as discussed in section 2. The model only considers perturbations that are sufficiently small compared to the corresponding non-perturbed basic state quantities. Its limitation therefore is that it cannot, in principle, describe the evolution of perturbations of finite magnitude that would evolve due to the nonlinear terms in Eqs. (7) and (14). Even so, the linearized model satisfactorily describes the wavelength of the dominant disturbance and its vertical structure, as well as to the e-folding time. We have also identified relatively well the level of minimum divergence in the region of 500 hPa, as well as the position of the steering level. The simplification applied us to address the problem of baroclinic instability in a strictly analytical way without resorting to numerical approximation. As the above shows, we have largely succeeded in this task. Similarly, using the p-system allowed us to work over the entire range of the atmosphere, and to use the natural boundary conditions at the upper and lower limits of the atmosphere, (whereas typical Eady-type models are formulated so that the upper boundary condition is defined at the upper boundary of the troposphere).

A clear disadvantage of this Eady-type model is the use of the f-plane approximation, i.e., the neglect of the variation of the Coriolis parameter with latitude. This is particularly evident in the instability of very long waves. In models of baroclinic instability that consider the latitude variable Coriolis parameter, for example through the β-plane approximation, very long waves are stabilized.

Potentially, it should be possible to further improve the model and to make it even closer to the conditions in the real atmosphere. If an entirely analytical solution is required, the energetics of and Eady-type model should be possible to incorporate into the framework of linearized equations. We also plan to do this as a part of further research. Separate effort could be devoted to introducing diabatic heating, surface friction, instability of nonzonal flow and/or finite amplitude instability (Pedlosky, 1987), and to other aspects, such as including a more realistic profile of wind speeds at mid-latitudes – some of the climatological reanalysis dataset could be used for this purpose. However, in these cases a strictly analytical approach would no longer be possible, and numerical methods would be required to reach the solutions.

It should also be noted that the normal modes method is not the only way to investigate baroclinic instability. Attention should also be paid to the nonmodal growth of perturbations, the classical concept of cyclogenesis in synoptic meteorology (Lackmann, 2011), or potential vorticity thinking (Holton, 2004).

Since we conclude this paper with an appendix on the choice of the mean value of the static stability parameter, let us also discuss in more detail the effect of the stability of the vertical atmospheric stratification on the growth rate of different long-wavelength disturbances. According to Dymnikov and Filatov (1990), the variation of the stratification in the lower atmosphere between 925 and 855 hPa mostly affects the stability of disturbances with wavelengths around 1,000 km. Stratification changes in mid-troposphere have significant effect on the growth rate of disturbances with wavelength of 2,000 to 3,000 km, but have no effect on shorter disturbances. Changes in the vertical stratification of the atmosphere at its highest levels have only a very weak effect on the growth rate of disturbances of all wavelengths.

APPENDIX

Let us investigate further the choice of the mean value of the atmospheric static stability parameter $\bar{\sigma}$. Assuming a temperature gradient $\frac{\partial T}{\partial z} = -0.0065\,Km^{-1}$ in the troposphere and substituting into the definition of the static stability parameter

$$\sigma \equiv -\frac{\alpha}{\theta}\frac{\partial \theta}{\partial p}$$

using the Poisson equation (definition of potential temperature), the equation of state, and the hydrostatic equilibrium equation, we get:

$$\sigma = \left(\frac{R}{p}\right)^2 \left(\frac{1}{c_p} - \frac{0.0065}{g}\right) T, \tag{A1}$$

$$\frac{\partial T}{\partial p} = \tilde{\kappa}\frac{T}{p}, \quad \text{where} \quad \tilde{\kappa} = 0.0065\frac{R}{g}.$$

Integrating the last equation, we get

$$T = T_0\left(\frac{p}{p_0}\right)^{\tilde{\kappa}},$$

which, after substitution into Eq. (A1), leads to the relation:

$$\sigma = a_1 T_0 p^{a_2},$$

where

$$a_1 = \frac{R^2}{p_0^{\tilde{\kappa}}}\left(\frac{1}{c_p} - \frac{0{,}0065}{g}\right)T,$$

$$a_2 = \tilde{\kappa} - 2.$$

T_0 is the temperature at the pressure level p_0 = 1000 hPa. The mean value $\bar{\sigma}$ in a certain region of the troposphere between the pressure levels p_1 and p_2 is obtained as follows:

$$\bar{\sigma} = \frac{a_1 T_0}{p_1 - p_2}\int_{p_1}^{p_2} p^{a_2}\,dp = \frac{a_1 T_0}{(p_1 - p_2)(a_2 + 1)}\left(p_1^{a_2+1} - p_2^{a_2+1}\right).$$

Using the last equation, we can easily verify that the value $\bar{\sigma} = 2 \cdot 10^{-6}\ m^2s^{-2}Pa^{-2}$, which we commonly use, represents the mean value of the atmospheric static stability parameter between the pressure levels 1,000 and 350 hPa and the temperature T_0 = 288 K at the 1,000 hPa level.

DATA ACCESSIBILITY STATEMENT

The source codes are available from http://www.doi.org/10.17605/OSF.IO/XH6S8.

FUNDING INFORMATION

This work has been funded partly by the project "Natural and Anthropogenic Georisks", No. CZ.02.01.01/00/22_008/0004605, funded within the Excellent Research call of the Johannes Amos Comenius Programme (P JAC).

COMPETING INTERESTS

The authors have no competing interests to declare.

AUTHOR CONTRIBUTIONS

A.R. designed the research, performed the calculations and wrote the manuscript. H.B. and J.M. supervised the research, and J.M. finalized the manuscript.

AUTHOR AFFILIATIONS

Aleš Raidl orcid.org/0000-0002-9766-975X
Department of Atmospheric Physics, Faculty of Mathematics and Physics, Charles University, Prague, Czech Republic

Hynek Bednář orcid.org/0000-0002-2045-1963
Department of Atmospheric Physics, Faculty of Mathematics and Physics, Charles University, Prague, Czech Republic

Jiří Mikšovský orcid.org/0000-0002-5259-2269
Department of Atmospheric Physics, Faculty of Mathematics and Physics, Charles University, Prague, Czech Republic

REFERENCES

American Meteorological Society. (2025) Rossby parameter, Glossary of Meteorology, https://glossary.ametsoc.org/wiki/Rossby_parameter

Bluestein, H.B. (1993) Synoptic-dynamic meteorology in midlatitudes, Vol II. Observations and theory of weather systems. Oxford University Press, Oxford.

Charney, J.G. (1947) The dynamics of long waves in a baroclinic westerly current. *Journal of Meteorology*, 4: 136–162. DOI: https://doi.org/10.1175/1520-0469(1947)004<0136:TDOLWI>2.0.CO;2

Charney, J.G. and **Stern, M.** (1962) On the stability of internal baroclinic jets in a rotating atmosphere. *Journal of Atmospheric Sciences*, 19(2): 159–172. DOI: https://doi.org/10.1175/1520-0469(1962)019<0159:OTSOIB>2.0.CO;2

Dutton, J.A. (1986) Dynamics of atmospheric motion: formerly the ceaseless wind. Dover Publications, New York.

Dymnikov, V.P. and **Filatov, A.N.** (1990) Stability of large-scale atmospheric processes. Gidrometeoizdat, Leningrad (in Russian).

Eady, E.T. (1949) Long waves and cyclone waves. *Tellus*, 1(3): 33–52. DOI: https://doi.org/10.3402/tellusa.v1i3.8507

Grotjahn, R. (1993) Global atmospheric circulations: observations and theories. Oxford University Press, New York.

Haltiner, G.J. and **Williams, R.T.** (1980) Numerical prediction and dynamic meteorology. 2nd ed., John Wiley & Sons.

Holton, J.R. (2004) An introduction to dynamic meteorology. 4th ed., Academic Press, Amsterdam, London.

Kalashnik, M.V. and **Chkhetiani, O.** (2018) An Analytical Approach to the Determination of Optimal Perturbations in the Eady Model. *Journal of the Atmospheric Sciences*, 2741–2761. DOI: https://doi.org/10.1175/JAS-D-18-0089.1

Lackmann, G. (2011) Midlatitude synoptic meteorology: dynamics, analysis, and forecasting. American Meteorological Society, Boston. DOI: https://doi.org/10.1007/978-1-878220-56-1

Mak, M. (2011) Atmospheric dynamics. Cambridge University Press, Cambridge.

North, G.R., Pyle, J. and **Zhang, F.** (eds). (2015) Encyclopedia of atmospheric sciences. 2nd ed., Academic Press.

Pedlosky, J. (1987) Geophysical fluid dynamics. 2nd ed. Springer-Verlag, New York. DOI: https://doi.org/10.1007/978-1-4612-4650-3

Stamper, M.A. and **Taylor, J.R.** (2017) The transition from symmetric to baroclinic instability in the Eady model. *Ocean Dynamics*, 67(1): 65–80. DOI: https://doi.org/10.1007/s10236-016-1011-6

Vic, A., Carton, X. and **Gula, J.** (2022) Eady Baroclinic Instability of a Circular Vortex. *Symmetry*, 14(7): 1438. DOI: https://doi.org/10.3390/sym14071438

TO CITE THIS ARTICLE:
Raidl, A., Bednář, H. and Mikšovský, J. 2025. Analytical Formulas for the Structure of Perturbations in the Eady Model of Baroclinic Instability in the *p*-System. *Tellus A: Dynamic Meteorology and Oceanography*, 77(1): 136–150. DOI: https://doi.org/10.16993/tellusa.4077

Submitted: 24 June 2024 **Accepted:** 03 April 2025 **Published:** 02 May 2025